Supporting Information

Molecular mechanism of enzymatic chlorite detoxification: insights from structural and kinetic studies

*Irene Schaffner[1‡], Georg Mlynek[2‡], Nicola Flego[3], Dominic Pühringer[2], Julian Libiseller-Egger[1], Leighton Coates[4], Stefan Hofbauer[1], Marzia Bellei[5], Paul G. Furtmüller[1], Gianantonio Battistuzzi[6], Giulietta Smulevich[3], Kristina Djinović-Carugo[2,7] and Christian Obinger[1]**

[1]Department of Chemistry, Division of Biochemistry, BOKU – University of Natural Resources and Life Sciences, Muthgasse 18, A-1190 Vienna, Austria

[2]Department for Structural and Computational Biology, Max F. Perutz Laboratories, University of Vienna, Dr.-Bohr-Gasse 9, A-1030 Vienna, Austria

[3]Dipartimento di Chimica "Ugo Schiff", Università di Firenze, Via della Lastruccia 3-13, I-50019 Sesto Fiorentino (FI), Italy

[4]Biology and Soft Matter Division, Oak Ridge National Laboratory, 1 Bethel Valley Road, Oak Ridge, Tennessee 37831, United States

[5]Department of Life Sciences, University of Modena and Reggio Emilia, Via Campi 103, 41125 Modena, Italy

[6]Department of Chemistry and Geology, University of Modena and Reggio Emilia, Via Campi 103, 41125 Modena, Italy

[7]Department of Biochemistry, Faculty of Chemistry and Chemical Technology, University of Ljubljana, 1000 Ljubljana, Slovenia

[‡]equally contributing first authors
*corresponding author
email: christian.obinger@boku.ac.at

S1 Experimental Section

4.1 Recombinant protein expression in *Escherichia coli* and purification by affinity chromatography

Chlorite dismutase from *Cyanothece* PCC7425 (CCld) was expressed and purified as described previously.[1] In short, Strep(II)-tagged CCld was recombinantly expressed in *E. coli* BL21 Gold (DE3) cells (Agilent). Cells were cultivated in LB medium supplemented with ampicillin (100 µg mL^{-1}). An overnight culture was used to inoculate fresh medium at a dilution ratio of 1:250. After the culture has reached an optical density at 600 nm of 0.6, hemin chloride (50 µg mL^{-1}) and isopropyl-β-D-thiogalactopyranoside (IPTG) (120 µg mL^{-1}) were added. Expression was carried out at 16°C overnight. Cells were harvested by centrifugation (5000 g, 20 min, 4°C). After resuspension in 50 mM HEPES pH 7.4, 5 % glycerol, 0.5 % Triton X-100, 0.5 mM EDTA and 1 mM phenylmethylsulfonylfluoride (PMSF), the cell pellet was lysed by ultra-sonication. After centrifugation (17000 g, 30 min, 4°C), the supernatant was applied to a StrepTrap HP 5 mL column (GE Healthcare) equilibrated with 20 mM HEPES pH 7.4 and 5 % glycerol. CCld was eluted from the column using 20 mM HEPES pH 7.4, 5 % glycerol and 1 mM d-desthiobiotin. Fractions containing CCld were pooled, concentrated and desalted using 10 kDa Amicon Ultra Centrifugal Filter (Millipore).

4.2 UV-vis spectroscopy and determination of K_D values

All UV-vis spectra were measured at room temperature on a Hitachi U-3900 spectrometer. For each measurement, 400 µL of CCld with a concentration of 5 µM were prepared in 50 mM potassium phosphate buffer (pH 5.8 - 11.5) and used for UV-vis analysis. Above pH 8.0, the desired pH values were adjusted with NaOH. Prior to each measurement, pH was checked carefully. Spectra were recorded in a wavelength range between 200-700 nm. For determination of the pK_a value, absorption values in the wavelength ranges 360.5-404.5, 414.5-449.5, 485.5-519.5, 540.5-559.5 and 620.5-644.5 nm were plotted against pH values. Resulting curves were fitted to the sigmoidal equation (a) and pK_a was obtained from x_0.

$$y = y_0 + \frac{a}{1+e^{-\frac{x-x_0}{b}}} \qquad \text{(a)}$$

To determine appropriate ligand concentrations for crystal soaking experiments, the dissociation constants of fluoride and thiocyanate were determined spectroscopically by ligand titration. Measurements were carried out in a quartz cuvette (d = 10 mm) in 0.1 M MES buffer, pH 6.5, using a Hitachi U3900 Spectrophotometer. CCld samples were diluted in MES buffer to a concentration of 10 µM in a starting volume of 500 µL and UV-vis spectra were recorded after stepwise addition of 400 mM ligand stock solutions of NaF or NaSCN under mixing. The wavelength range was set to 250-700 nm with a scan speed of 300 nm/min at a sampling rate of 0.5 nm. The sampled concentration ranges for the ligands were 0.008-

162 mM for NaF and 0.008-13.060 mM for NaSCN. From the obtained spectra, the absorption values at 611 nm for NaF and 414 nm for NaSCN were plotted against the ligand concentrations and the resulting curves were fitted by least squares regression to the rectangular hyperbolic equation b.

$$y = y_0 + \frac{a*x}{b+x} \qquad (b)$$

4.3 X-ray crystallographic studies

To ensure optimal prerequisites for structural studies, all experiments were carried out using tag-free enzyme. In order to remove the Strep(II)-tag, CCld was incubated overnight at 4°C with ten-fold excess of human rhinovirus 3C protease fused to glutathione-S-transferase (GST-tag). The digested sample was then loaded onto in series connected GSTrap HP column (to retain the protease), StrepTrap HP column (to remove the cleaved tag and uncleaved protein) and a HiLoad 16/60 Superdex prep grade column (final polishing step). All columns were purchased from GE Healthcare. Finally, the protein solution was concentrated to approximately 7 mg mL^{-1} using 10 kDa Amicon Ultra Centrifugal Filter. Initial CCld crystallization experiments were done using the vapor diffusion method. Crystallization drops were set using a Phoenix HT crystallization robot (Art Robins Instruments). Ratios of 150:200 nL, 200:200 nL and 250:200 nL protein to crystallant were dispensed. Commercially available crystallization screens were used for initial screening. Hits were obtained using JCSG-plusTM from Molecular Dimensions and Crystallization Screen from Hampton Research. Further optimization yielded the working crystallization conditions (0.15 M $MgSO_4$, 0.1 M MES pH 6.5, 22% w/v PEG 3350, 5% glycerol and 0.2 M $MgCl_2$, 0.1 M TRIS-HCl pH 8.5, 20% w/v PEG 4000). Crystallization plates were stored in and imaged with a Minstrel DT UV device (Rigaku) at 22°C. Obtained crystals were soaked with mother liquor supplemented with 20% 2-methyl-2,4-pentanediol (MPD) as cryoprotectant. Data sets for CCld were collected at beam-lines ID23-2 (pH 8.5) and ID30b (pH 6.5) of European Synchrotron Radiation Facility (ESRF, France) at 100 K. For CCld in complex with SCN^-, the protein solution was mixed with NaSCN to reach a final ligand concentration of 10 mM. Data sets for CCld in complex with SCN^- were collected at beam-line ID02 of Diamond Light Source (Great Britain) at 100 K. For CCld in complex with fluoride, the crystallization solution was supplemented with 200 mM NaF. Data sets were collected at beam-line ID23-1 of ESRF at 100 K. All data sets were processed with XDS and converted with XDSCONV.[2] The phase problem of CCld at pH 8.5 was solved by molecular replacement using Phaser-MR[3] taking pdb structure 3QPI (dimeric chlorite dismutase from *Nitrobacter winogradskyi*). We further used this structure to solve the phase problem of CCld at pH 6.5, CCld in complex with SCN^- and CCld in complex with F^-.

The model was further improved by iterative cycles of manual model building using COOT[4] and maximum likelihood refinement using PHENIX-Refine. For CCld in complex with fluoride, anisotropic ADP refinement for proteins, ligands and waters was performed. For CCld in complex with isothiocyanate, CCld at pH 6.5 and pH 8.5, anisotropic ADP refinement for proteins and ligands was

performed. Final stages of refinement included automated addition of hydrogens and water molecules, optimization of X-ray/ADP weight and optimization of X-ray/stereochemistry weight. The model was validated with MolProbity[5] and PDBREDO[6]. The high resolution cutoff was based on performing paired refinement using the PDB-REDO webserver.[7] Final refinement statistics are shown in Table 1 and Supplemental Table 3. Figures were prepared with PyMOL.[8] RMSD values were calculated using PyMOL. Atomic coordinates have been deposited in the Protein Data Bank under accession codes 5MAU (H_2O bound CCld), 5K8Z (OH^- bound CCld), 5K90 (CCld in complex with SCN^-) and 5K91 (CCld in complex with F^-).

4.4 Neutron crystallography

To grow CCld crystals to appropriate size for neutron diffraction (i.e. ~1 mm^3), the technique of capillary counter diffusion was used[9]. Quartz capillaries were purchased from VitroCom and had an inner diameter of 1.5 mm and an outer diameter of 1.8 mm. They were cut to a size of 60 mm. Each capillary was filled with 30 µL of crystallization solution and 30 µL of protein solution (8 mg/mL) which were separated by a 1% agarose plug of approx. 10 mm length acting as diffusion barrier. Crystallization solution contained 0.1 M MES pH 6.5, 0.15 M $MgSO_4$, 30% PEG 3350 and 5% glycerol.

Crystal growth was promoted by applying the micro seeding technique which allows growth of larger single crystals in the metastable zone by providing nucleation seeds. In detail, a seeding stock solution was prepared using the Seed Bead™ kit of Hampton Research. For that, one single crystal was placed into 50 µL crystallization solution, crushed and finally transferred into a Seed Bead™ tube. The solution was vortexed 3 × 30 s cooling it on ice between the mixing steps. Seeding stock was added to fresh protein solution in a ratio of 1:100 immediately before loading the capillary. Capillaries were sealed using capillary wax from Hampton Research. To prepare the obtained crystal for data collection, all components of the crystallization solution (0.1 M glycine-NaOH pH 9.0, 0.15 M $MgSO_4$, 30% PEG 3350, 5% glycerol) were dissolved in D_2O. Note that the desired pH (i.e. pH 9.0) was adjusted at this step of crystal preparation. Hydrogenated precipitant solution was then removed from the capillary and replaced by deuterated crystallization solution which was placed directly against the agarose plug, allowing free liquid diffusion. This process was repeated at least three times over the course of one week.

Time of flight (TOF) neutron diffraction data of CCld at pD 9.4 were recorded from an approx. 1 mm^3 crystal using the MaNDi instrument [10,11] located at the Spallation Neutron Source (SNS) at Oak Ridge National Laboratory (ORNL). Data collection was performed at 293 K. In total, 26 images were collected (with an average exposure time of 18 h per image) from 26 different crystal orientations. Immediately after neutron data collection, an X-ray diffraction data set was recorded at 293 K on the same crystal using an in house Rigaku MM007-HF X-ray generator equipped with a RAXIS IV++ detector. X-ray data were

processed using the XDS package[2]. Neutron data were processed using the Mantid package[12] and the Lauenorm program from the Lauegen package[13].

The studied crystal was isomorphous to a previously solved X-ray structure of CCld. This structure was used as a starting point for structural refinement using the PHENIX software suite.[3] To start with, the model was refined against X-ray data alone, followed by joint X-ray and neutron refinement[14,15]. H- and D-atoms were added with the program ReadySet. As the protein was not perdeuterated, all non-exchangeable hydrogen atoms were ^{1}H. H_2O molecules were replaced with D_2O using a text editor. After the first refinement, all D_2O positions were checked according to peaks in the $2F_o$-F_c nuclear density map and to positive and negative peaks in the F_o-F_c difference map and required modifications were done using the software COOT[4]. Final refinement statistics are shown in Table 1 and Supplemental Table 3. Atomic coordinates have been deposited in the Protein Data Bank under accession codes 5NKU for CCld structure refined against joint X-ray/neutron data and 5NKV for the structure refined against X-ray data only.

4.5 Resonance Raman spectroscopy

The resonance Raman spectra were obtained at 25°C using a 5 mm NMR tube by excitation with the 413.1 nm line of a Kr^+ laser (Coherent, Innova 300 C, Coherent, Santa Clara, CA, USA) and with the 441.6 nm line of a He–Cd laser (Kimmon IK4121R-G). Backscattered light from a slowly rotating NMR tube was collected and focused into a triple spectrometer (consisting of two Acton Research SpectraPro 2300i instruments and a SpectraPro 2500i instrument in the final stage with gratings of 3600 grooves/mm and 1800 grooves/mm) working in the subtractive mode, equipped with a liquid nitrogen-cooled CCD detector. A spectral resolution of 1.2 cm^{-1} and spectral dispersion of 0.40 cm^{-1}/pixel were calculated theoretically on the basis of the optical properties of the spectrometer for the 3600 grating; for the 1800 grating, used to collect the RR spectra of the ferrous CO complexes in the 1700–2300 cm^{-1} region, the spectral resolution was 4 cm^{-1} and spectral dispersion 1.2 cm^{-1}/pixel. The RR spectra were calibrated with indene, n-pentane, dimethylsulphoxide, acetonitrile and carbon tetrachloride as standards to an accuracy of 1 cm^{-1} for intense isolated bands. All RR measurements were repeated several times under the same conditions to ensure reproducibility. Absorption spectra with a double-beam spectrophotometer (Varian Cary 5), using a 5-mm NMR tube and a 600 nm/min scan rate were measured both prior to and after RR measurements to ensure that no degradation had taken place under the experimental conditions used. No changes have been observed within 30 min of irradiation with 5 mW (ferric) and 10 mW (ferrous) for laser excitation in the Soret band. To improve the signal-to-noise ratio, a number of spectra were accumulated and summed only if no spectral differences were noted. All spectra were baseline-corrected. To determine peak bandwidth and positions, a curve-fitting program (Lab Calc; Galactic) was used to simulate the spectra using a Lorentzian line shape. The frequencies of the bands were optimized with an accuracy of 1

cm^{-1} and the bandwidths with an accuracy of 0.5 cm^{-1}. Bandwidth (full width at half-maximum) of the bands in the low frequency was in general 13 cm^{-1}; the bands at 489.5 (γ_{22}) and 507 (γ_{12}) were 18 and 17 cm^{-1}, respectively (See Supplemental Table 1).Buffered solutions (0.1 M) were used for experiments at pH 9.6 - 10.1 (glycine), 7.0 (phosphate), and ca. 6 (MES). Protein concentrations in the range 25 – 60 μM were used for the electronic absorption and RR samples. The ferrous form was obtained by adding a small volume (2 μL) of a fresh sodium dithionite solution (10 mg/mL) to 50 μL of a deoxygenated protein solution. The CO complexes were prepared by degassing the ferric protein solution by flushing firstly with nitrogen, then with CO or ^{13}CO and reducing the heme by addition of a 5% volume freshly prepared sodium dithionite (10 mg/mL) solution.

The hydroxyl complex in isotopically enriched water was prepared by adding 5 μL of CCld, in 0.02 M natural abundance buffer, to 50 μL of 0.1 M glycine buffer prepared with D_2O or $H_2{}^{18}O$ to obtain a final pD 10.1 and pH 9.6, respectively.

Phosphate salts and glycine were obtained from Merck AG (Darmstadt, Germany). 2-[N-morpholino]ethanesulfonic acid (MES) was bought from Sigma-Aldrich (Steinheim, Germany). Gaseous ^{12}CO and ^{13}CO were purchased from Rivoira and FluoroChem, respectively. Sodium dithionite was obtained from Fluka. Isotopically enriched water ($H_2{}^{18}O$) (95%) and D_2O (99.8%) was purchased from Cambridge Isotope Laboratories (USA) and Merck AG (Darmstadt, Germany), respectively. All chemicals were of analytical or reagent grade and were used without further purification.

4.6 Spectroelectrochemistry

The standard reduction potential, *E*°', of the Fe(III)/Fe(II) couple was determined using a homemade OTTLE (optical transparent thin-layer spectroelectrochemical) cell[16-18]. The three-electrode configuration consisted of a gold minigrid working electrode (Buckbee-Mears), a homemade Ag/AgCl/KCl_{sat} microreference electrode, separated from the working solution by a Vycor set, and a platinum wire as the counter electrode. The reference electrode was calibrated against a saturated calomel (HgCl) electrode before each set of measurements. All potentials are referenced to the SHE (standard hydrogen electrode, 242 mV). Potentials were applied across the OTTLE cell with an Amel model 2053 potentiostat/galvanostat. A constant temperature was maintained by a circulating water bath and the OTTLE cell temperature was monitored with a copper-costan microthermo-couple. UV-vis spectra were recorded using a Varian Cary C50 spectrophotometer. The OTTLE cell was flushed with argon gas to establish an oxygen-free environment in the cell. The standard reduction potential was determined at pH 5.0, 6.0, 7.0 and 10.0. In the acidic to neutral pH range, 100 mM potassium phosphate buffer plus 100 mM NaCl was applied. At alkaline pH, 100 mM glycine-NaOH buffer plus 100 mM NaCl was used. Every measurement was carried out using 22 μM CCld. 400 μM methyl viologen as well as a mixture of 2 μM

lumiflavine-3-acetate, methylene blue, phenazine methosulfate and indigo disulfonate were used as mediators.

4.7 Polarographic measurement of O_2 generation

Reaction of CCld with chlorite or hypochlorite was followed polarographically using a Clark-type oxygen electrode (Oxygraph plus, Hansatech Instruments Ltd, Norfolk, United Kingdom). Temperature was held constant at 30°C. The electrode was calibrated to 100% O_2 saturation by flushing with oxygen and to 0% O_2 by flushing with nitrogen. Reaction mixtures contained 150 mM potassium phosphate buffer (pH 5.0 and 7.0) or 25 mM glycine/NaOH buffer (pH 9.0), 40 µM hypochlorite (ε_{292nm}=350 M^{-1} $cm^{-}1$; diluted in 5 mM NaOH due to its instability at acidic conditions[19]) or 20 µM chlorite (ε_{260nm}=155 M^{-1} cm^{-1}) and 1.5 µM CCld. To determine the amount of oxygen that is introduced to the system by applying the starting solution, the reaction mixture was prepared without substrate.

4.8 Stopped-flow spectroscopy

All UV-vis stopped-flow spectroscopy measurements were carried out on an instrument equipped for both, conventional and sequential measurements (model SX-18MV, Applied Photophysics) as well as with a diode array detector (Applied Photophysics). The optical quartz cell had a path length of 10 mm and a volume of 20 µL. All experiments were conducted at 25°C. Time-resolved spectra were recorded after a minimum dead time of 1 ms. For all measurements, a final concentration of 1.5 µM CCld in 150 mM potassium phosphate buffer (pH 5.0, 6.0, 7.0, 8.0) and in 25 mM glycine/NaOH buffer (pH 9.0, 9.6) was applied. Cyanide was used at concentrations ranging from 15-250 µM. To determine the pseudo-first-order rate constants, k_{obs}, either the decrease in absorbance at 405 nm was fit single exponentially (pH 5.0, 6.0, 7.0) or the increase in absorbance at 410 nm or 423 nm was fit double exponentially (pH 8.0, 9.0, 9.6). Hypochlorite was applied at concentrations from 8-49 µM (pH 5.0 and 7.0) or 500 µM (pH 9.0). k_{obs} values were determined by fitting the time trace at 405 nm to a single exponential. A chlorite concentration of 500 µM was used for recording spectra at pH 5.0, 7.0 and 9.0. All measurements were performed at least in duplicates. The apparent second-order rate constants for binding of cyanide and generation of Compound I with hypochlorite were obtained from the slope of a plot of k_{obs} versus the concentrations of the respective ligand and reactant. For cyanide, a plot of k_{on} *versus* pH was generated and the curve was fit to the equation c.

$$y = \frac{a}{1+\frac{b}{x}} \qquad \text{(c)}$$

S2 Supporting Figures

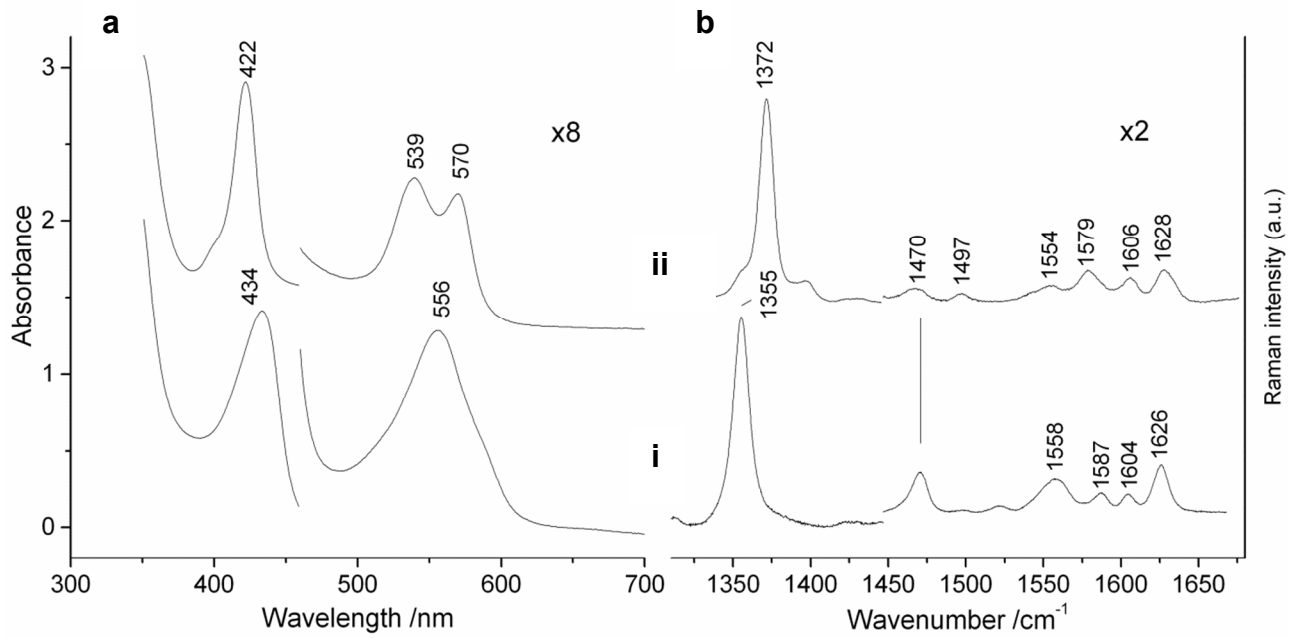

Figure S1. Comparison of (a) electronic absorption and (b) high frequency RR spectra of ferrous CCld (i) and its Fe(II)-CO complex (ii) at pH 5.8; Experimental conditions: (a): 600 nm /min scan rate. The region between 450 nm and 700 nm has been expanded 8-fold. (a): (a) 441.6 nm exc.,11 mW laser power at the sample, average of 2 spectra with 20 min integration time; (b) 413.1 nm exc., 5 mW laser power at the sample, average of 5 min integration time; The region between 1450 and 1700 cm^{-1} has been expanded 2-fold. The intensity of the spectra is normalized to that of the ν_4 band.

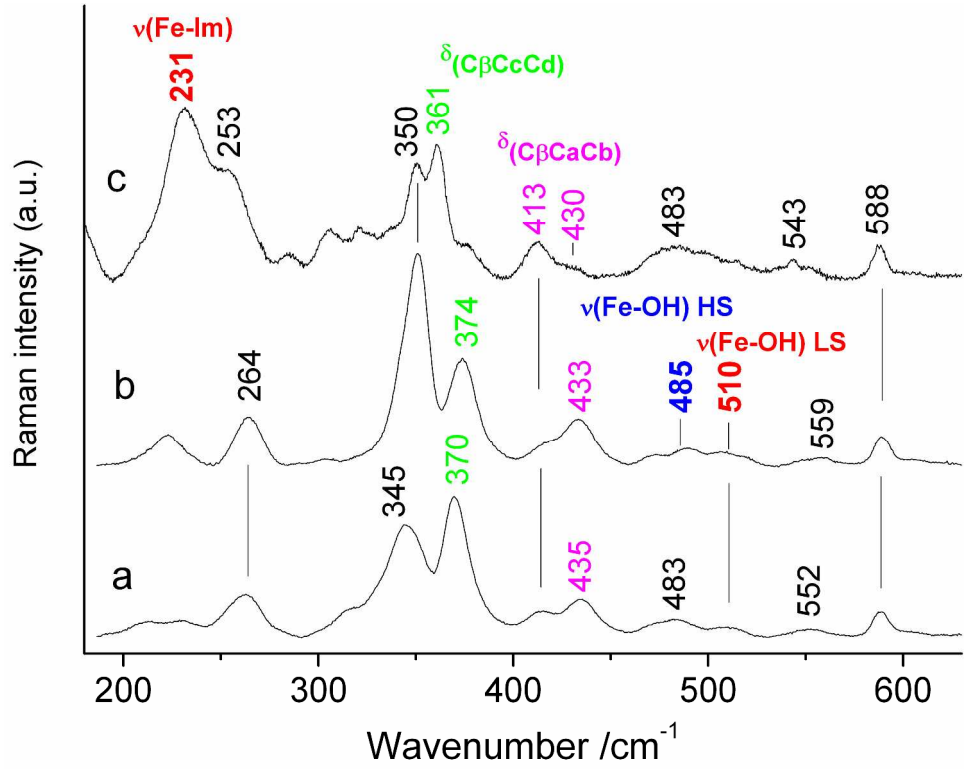

Figure S2. Low frequency RR spectra of ferric (pH 5.9) (a), pH 9.6 (b), and ferrous CCld (pH 5.8) (c); Experimental conditions: (a,b): 413.1 nm exc.,5 mW laser power at the sample; (a) average of 4 spectra with 40 min integration time; (b) average of 12 spectra with 120 min integration time; (c) 441.6 nm exc., 11 mW laser power at the sample, and average of 2 spectra with 20 min integration time. The spectra have been shifted along the ordinate axis to allow better visualization.

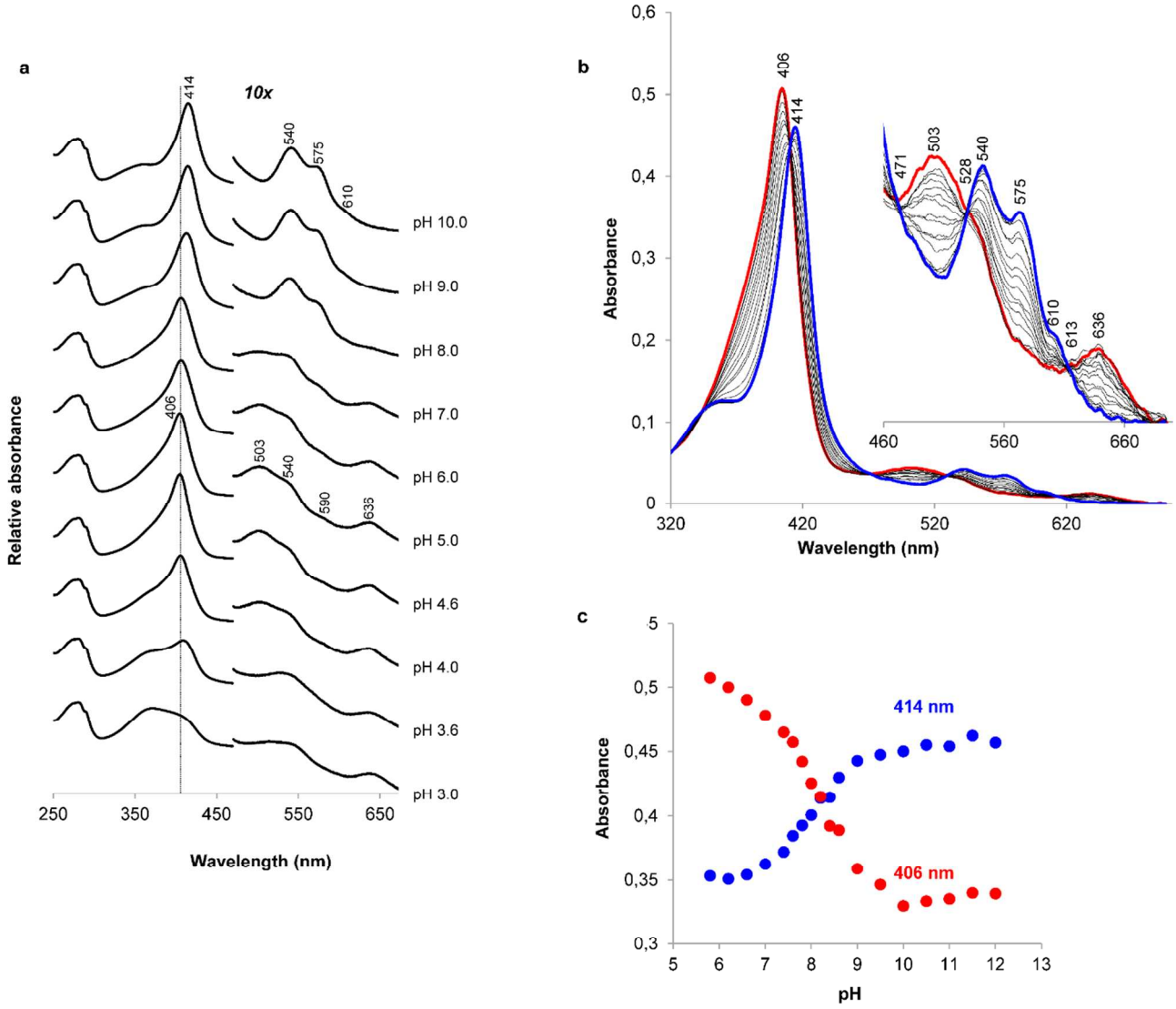

Figure S3. pH-dependent UV-vis spectral changes of CCld. (a) UV-vis spectra recorded in the pH range from pH 3.0 to pH 10.0. For measurements at acidic and neutral pH (3.0 to 7.0) 50 mM citrate phosphate buffer was used. In the alkaline pH range (8.0 to 10.0) 50 mM glycine-NaOH buffer was used. For better visualization of the CT and Q bands, the 460-700 nm region is magnified 10-fold. **(b)** CCld samples were prepared in 50 mM potassium phosphate buffer. For measurements above pH 8.0, buffer was adjusted with NaOH. Prior to each measurement, the pH of the protein solution was checked. For better visualization of the CT and Q bands, the spectra are depicted as an inset in the wavelength range between 460 nm and 700 nm. Peak maxima as well as isosbestic points are labelled. **(c)** Increase and decrease in absorbance with changing pH at 414 nm and 406 nm, respectively.

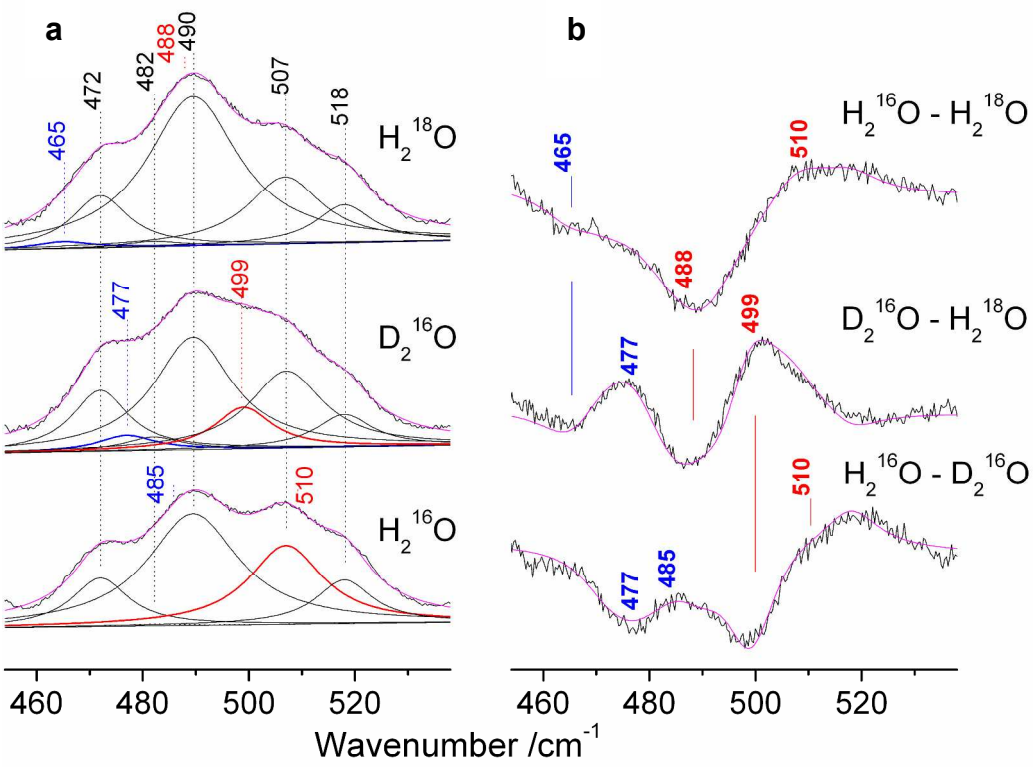

Figure S4. (a) RR spectra of ferric CCld (pH 9.6) in H_2O, D_2O and $H_2{}^{18}O$ buffered solutions, obtained with 413.1 nm exc., 5 mW laser power at the sample, and average of 12 spectra with 120 min integration time. The individual fitting components are displayed as solid black lines, except for the LS (HS) ν(Fe-OH) component shown as red (blue) lines. The spectra have been shifted along the ordinate axis to allow better visualization. **(b)** Difference spectra between the experimental (black) and fitted (magenta) spectra. The Fe-hydroxide LS (HS) frequencies are indicated in red (blue).

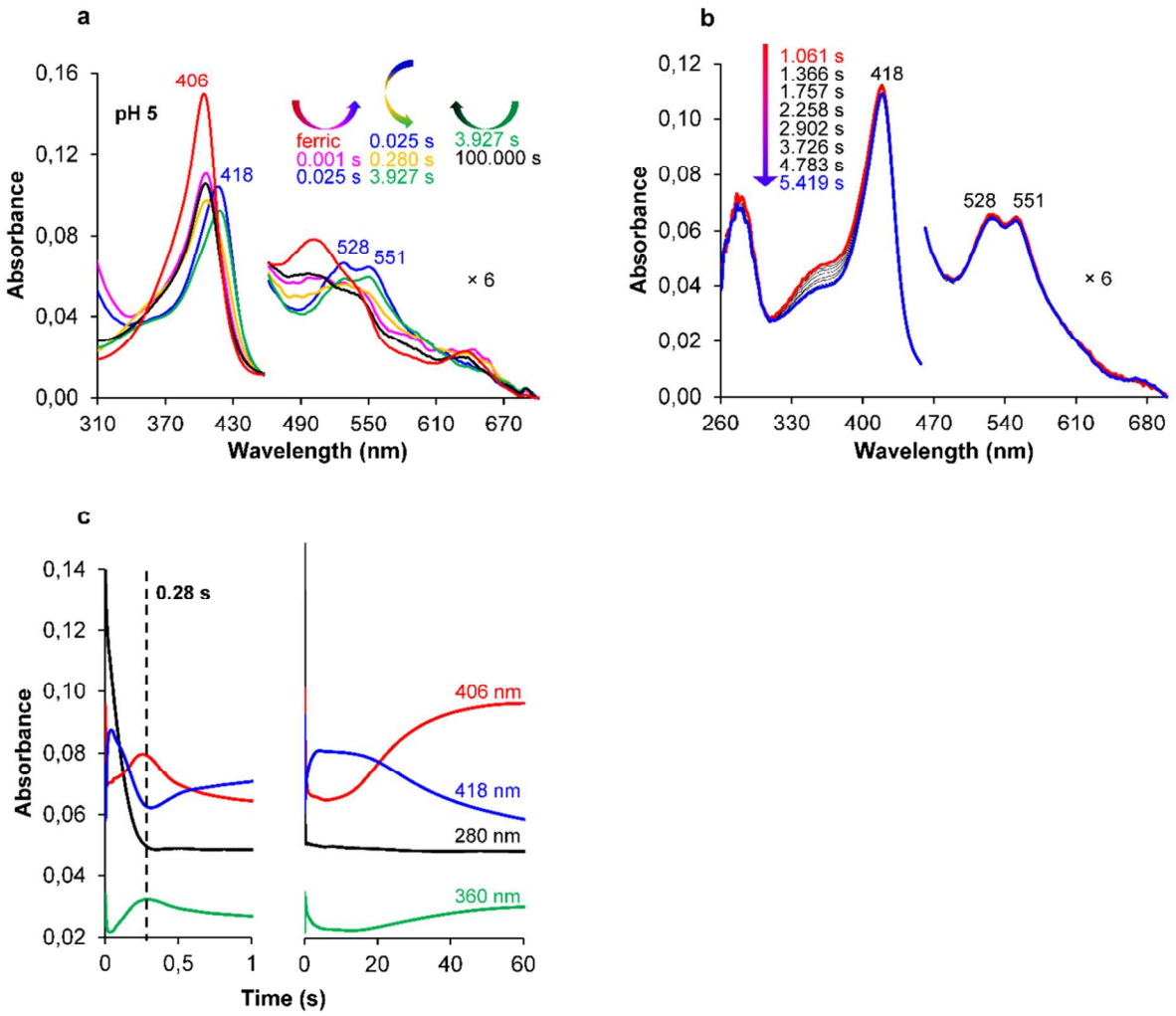

Figure S5. Reaction of ferric CCld with chlorite at pH 5.0. (a) Spectral changes of 1.5 µM CCld upon reaction with 1000 µM chlorite at pH 5.0. Spectrum of ferric CCld is shown in red, the dominating Compound II intermediate spectrum is depicted in blue. Peak maxima are labelled. For better visualization of the CT and Q bands, the 460-700 nm region is magnified 6-fold. Arrows indicate the course of the reaction by both, their colors and directions. **(b)** Spectral indication of chlorine dioxide (ClO_2) degradation by CCld. Change of UV-vis spectra of 1.5 µM CCld between 1.061 s (red) to 5.419 s (blue) after mixing with 1 mM chlorite at pH 6.0. The Soret as well as the visible region of the spectra remain unaltered whereas a significant hypochromocity at 360 nm, indicative of ClO_2 degradation, can be observed. **(c)** Time traces of the reaction depicted in (a). 405 nm: ferric Soret maximum, red; 418 nm: Soret maximum of the dominating Compound II intermediate species, blue; 280 nm: chlorite decomposition, black; 360 nm: chlorine dioxide decomposition, green. To visualize the correlations between chlorite degradation and chlorine dioxide formation (until 0.28 s) and between degradation of the latter and the enzyme adopting a second time the Compound II-like state (after 0.28 s), the appropriate time frame is displayed in the left part of (c).

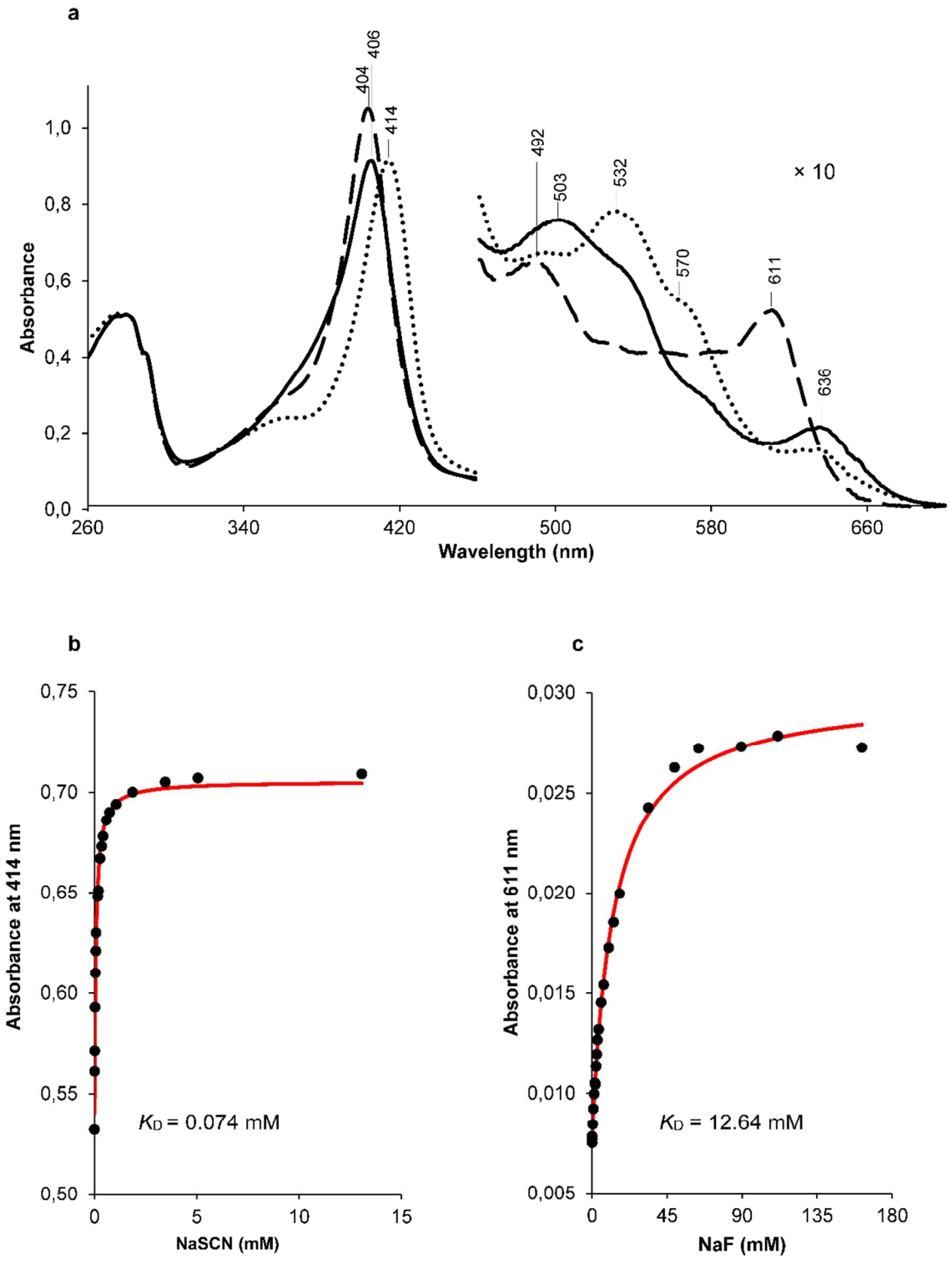

Figure S6. Binding of isothiocyanate and fluoride to CCld followed by UV-vis spectroscopy. (a) fluoride: dashed line, isothiocyanate: dotted line, no exogenous ligand: bold line. **(b, c)** Absorbance dependence upon ligand concentration at single wavelengths (i.e. 611 nm for F^- and 414 nm for SCN^-) which were chosen due to the distinct difference in absorption intensity of the unbound and bound state.

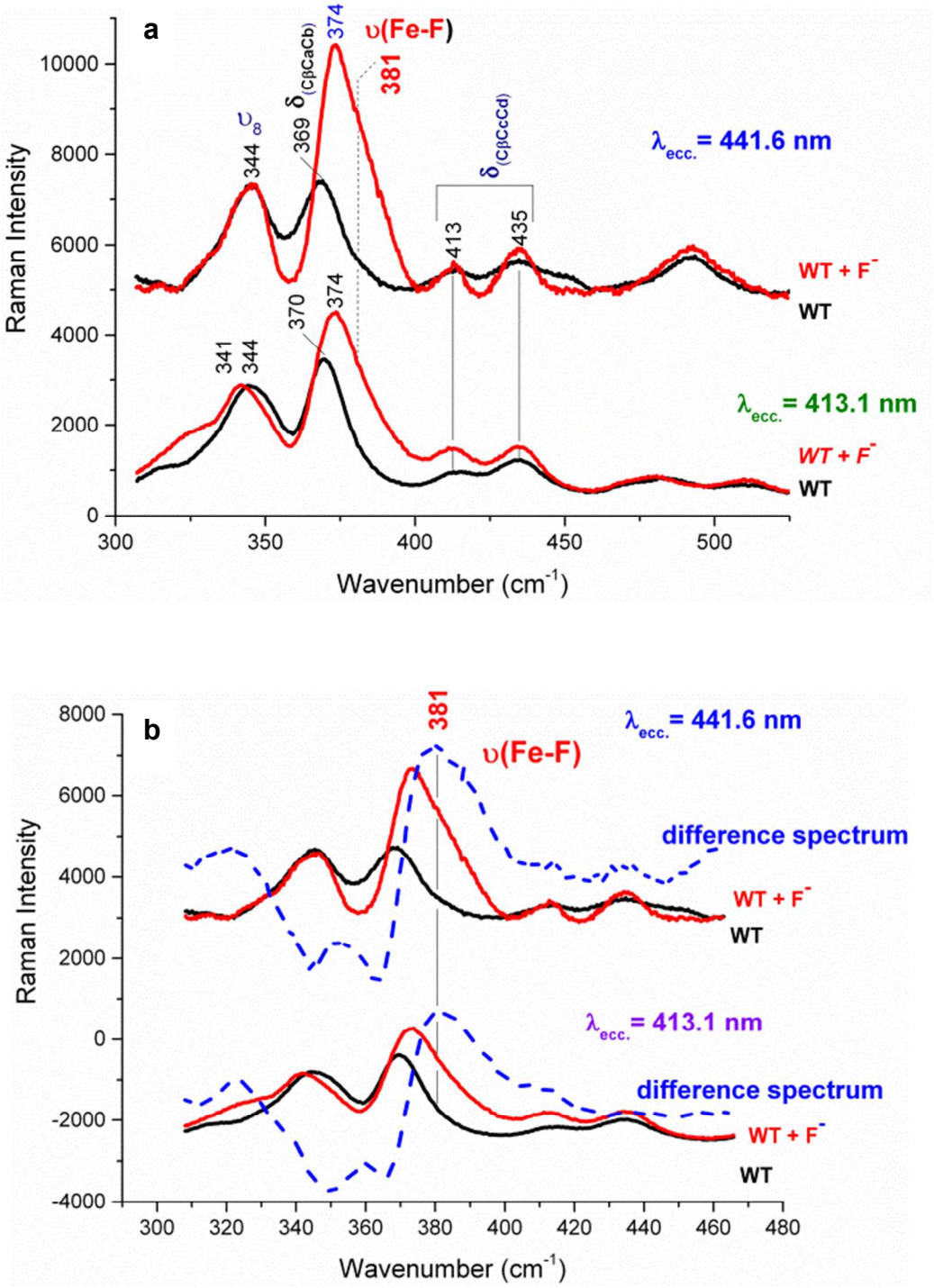

Figure S7. (a) Comparison of the RR spectra of CCld with (blue) and without (red) fluoride in the low frequency region taken with excitation in resonance with the Soret (413.1 nm) and with the CT2 band (441.6 nm). Spectra have been shifted along the ordinate axis to allow better visualization. Experimental conditions: (413.1 nm): 5 mW laser power at the sample, 40 min integration time. (441.6 nm): 25 mW laser power at the sample, 60 min integration time. The spectra are normalized on the band at 344 cm^{-1} (ν_8). **(b)** WT-F^- minus WT difference spectra in the low frequency region taken with excitation in resonance with the Soret (413.1 nm) and with the CT2 band (441.6 nm). The positive band at 381 cm^{-1} is assigned to the ν(Fe-F) stretching mode.

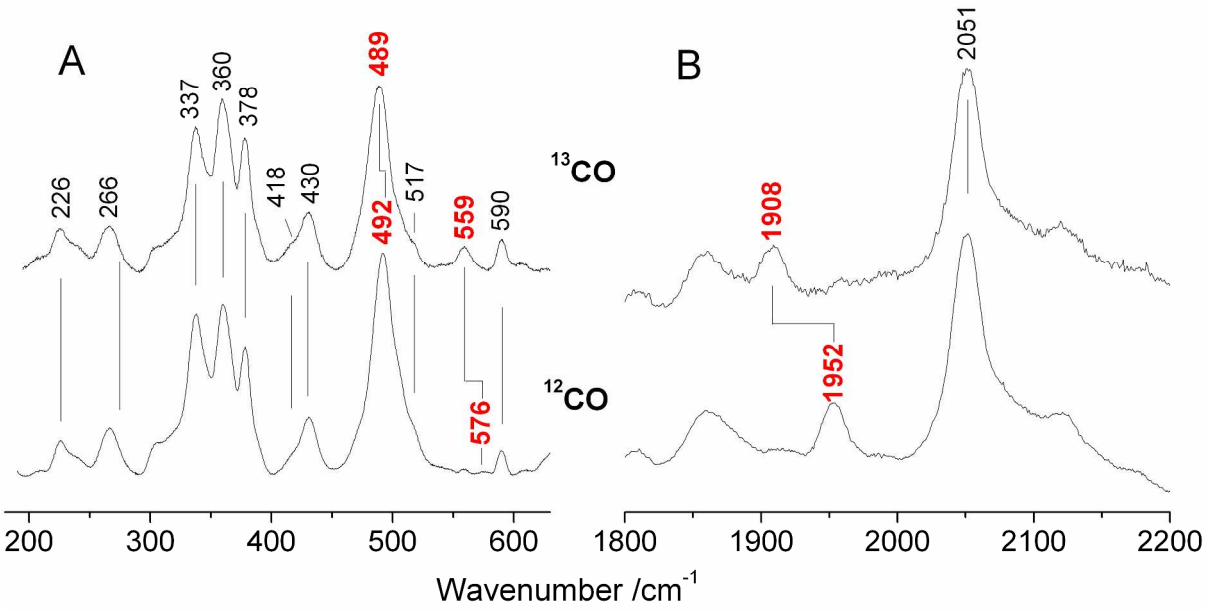

Figure S8. RR in the low **(a)** and high **(b)** frequency of the ^{12}CO and ^{13}CO complexes of the ferrous CCld-CO complex at pH 5.8 obtained with 413.1 nm exc. and 5 mW laser power at the sample. The ν(Fe-CO) and ν(C-O) stretching modes are indicated in red. (a) (^{12}CO) average of 4 spectra with 40 min integration time and (^{13}CO) of 3 spectra with 30 min integration time; the intensity of the spectra is normalized to that of the band at 590 cm^{-1}(ν_{48}); (b) (^{12}CO) average of 3 spectra with 30 min integration time and (^{13}CO) of 4 spectra with 40 min integration time; the intensity of the spectra is normalized to that of the band at 2051 cm^{-1}. The spectra have been shifted along the ordinate axis to allow better visualization.

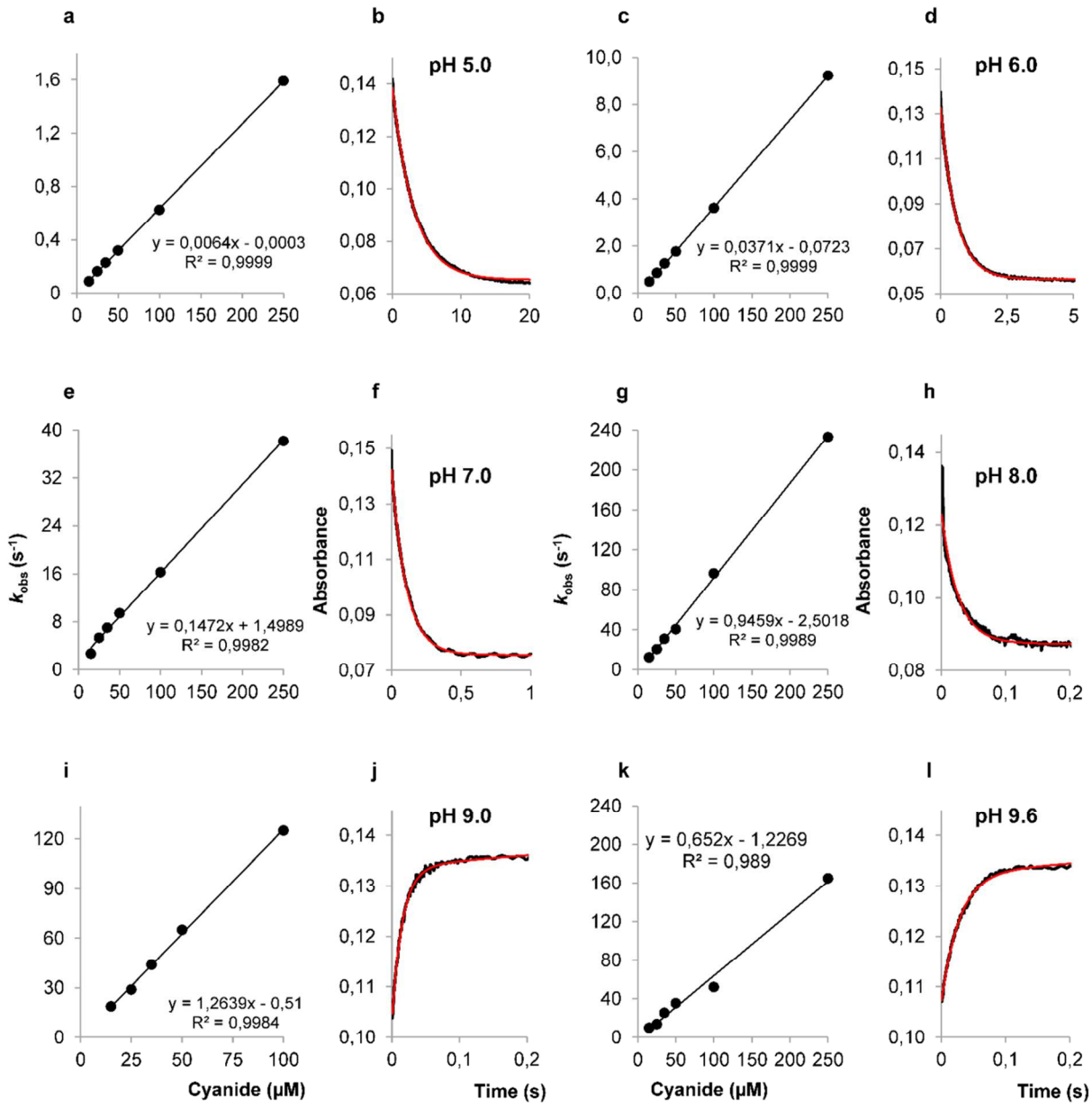

Figure S9. Binding of cyanide to ferric CCld at pH 5.0 **(a, b),** 6.0 **(c, d),** 7.0 **(e,f),** 8.0 **(g, h),** 9.0 **(i, j)** and 9.6 **(k, l)** followed by UV-vis stopped-flow spectroscopy. **(a, c, e, g, i, k)** Plots of k_{obs} *versus* cyanide concentration. The apparent association constant k_{on} was obtained from the slope of the regression line. **(b, d, f, h, j, l)** Typical time traces at 405 nm (b, d, f), 410 nm (h) and 423 nm (j, l) upon binding of cyanide to CCld (black) and single exponential (b, d, f) and double exponential (h, j, l) curve fit (red).

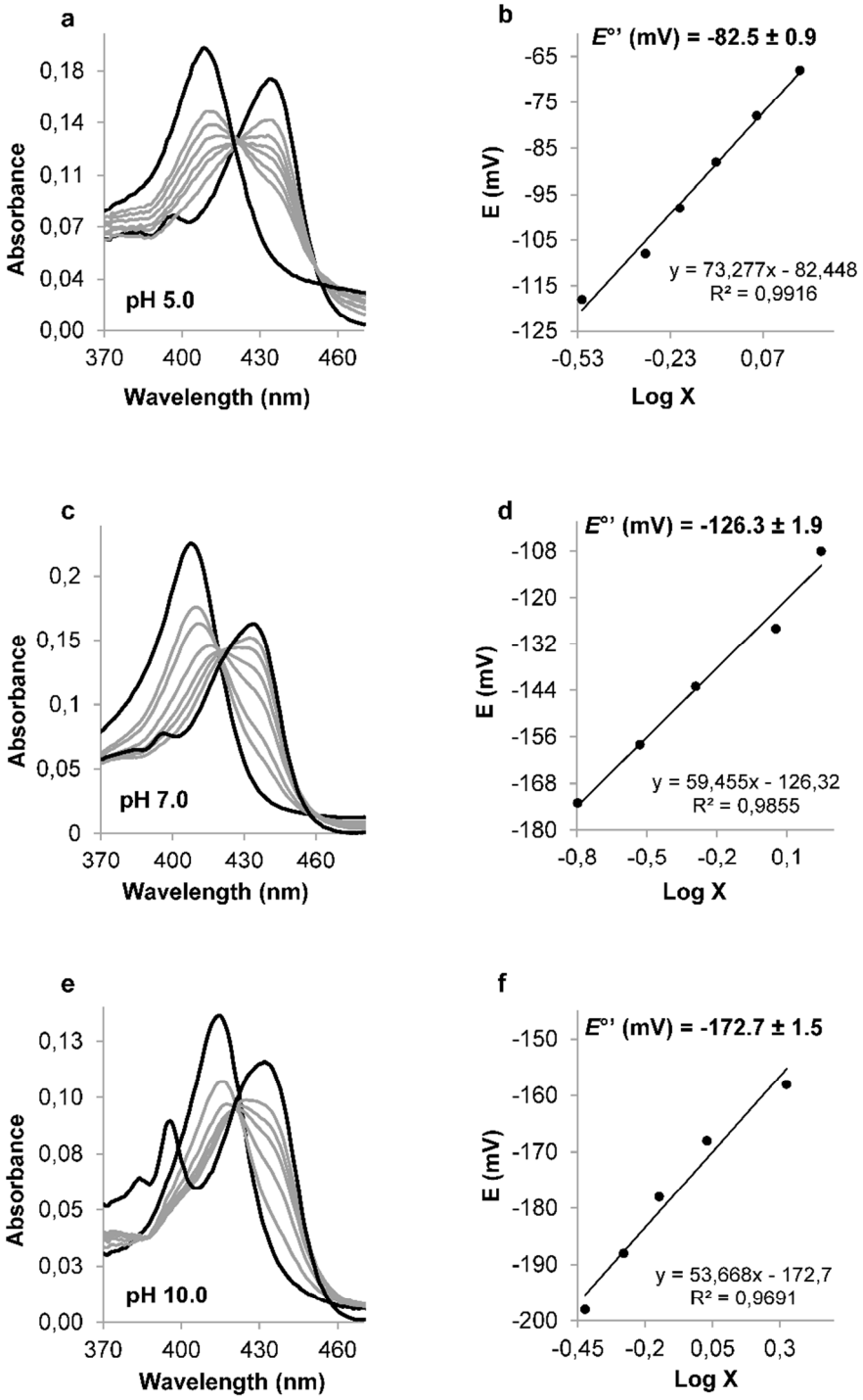

Figure S10. Spectroelectrochemical titration of the Fe(III)/Fe(II) redox couple of the high-spin native form of CCld at various pH values. (a, c, e) Electronic absorption spectra of CCld at pH 5.0, 7.0 and 10.0, respectively, and at different applied potentials. Black lines represent the fully oxidized ($A_{\lambda ox}^{Max}$ at 407 nm) and fully reduced form ($A_{\lambda red}^{Max}$ at 434 nm) for measurements at pH 5.0 and 7.0, respectively. At pH 10.0, $A_{\lambda ox}^{Max}$ and $A_{\lambda red}^{Max}$ were at 414 nm and 434 nm, respectively. (**b, d, f)** Corresponding Nernst plots for measurements at pH 5.0, 7.0 and 10.0, respectively, where X represents $(A_{\lambda red}^{Max} - A_{\lambda red})/(A_{\lambda ox}^{Max} - A_{\lambda ox})$.

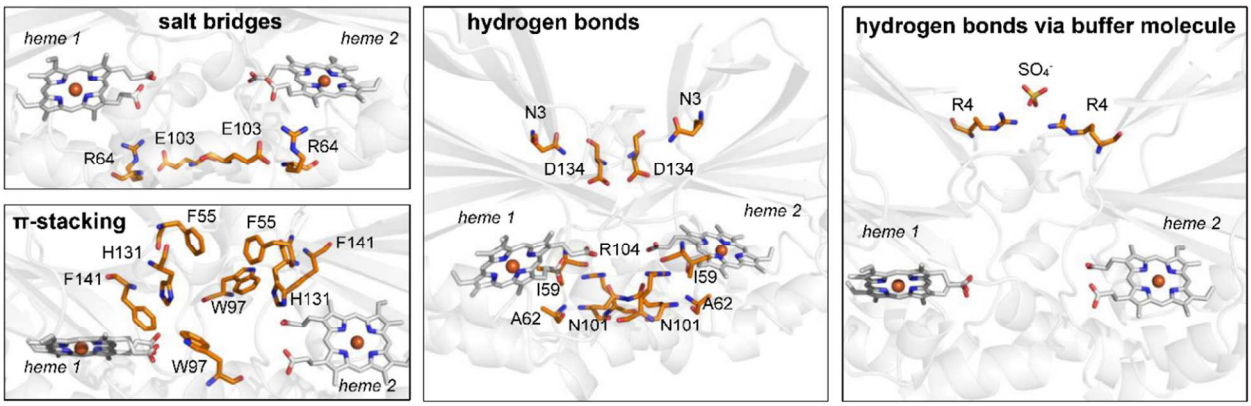

Figure S11. Non-covalent interactions between dimer interface residues identified by the RING 2.0 server using default settings[20]. Amino acid residues involved in salt bridges (R64-E103), hydrogen bonds (N3-D134, I59-R104, A62-N101, R4-SO_4^-) and π-stacking (W97-F141-H131-F55-F55-H131-F141-W97) are displayed as orange sticks. For facilitated orientation, heme groups of both subunits are displayed as grey sticks. The figure was prepared using PyMOL[8].

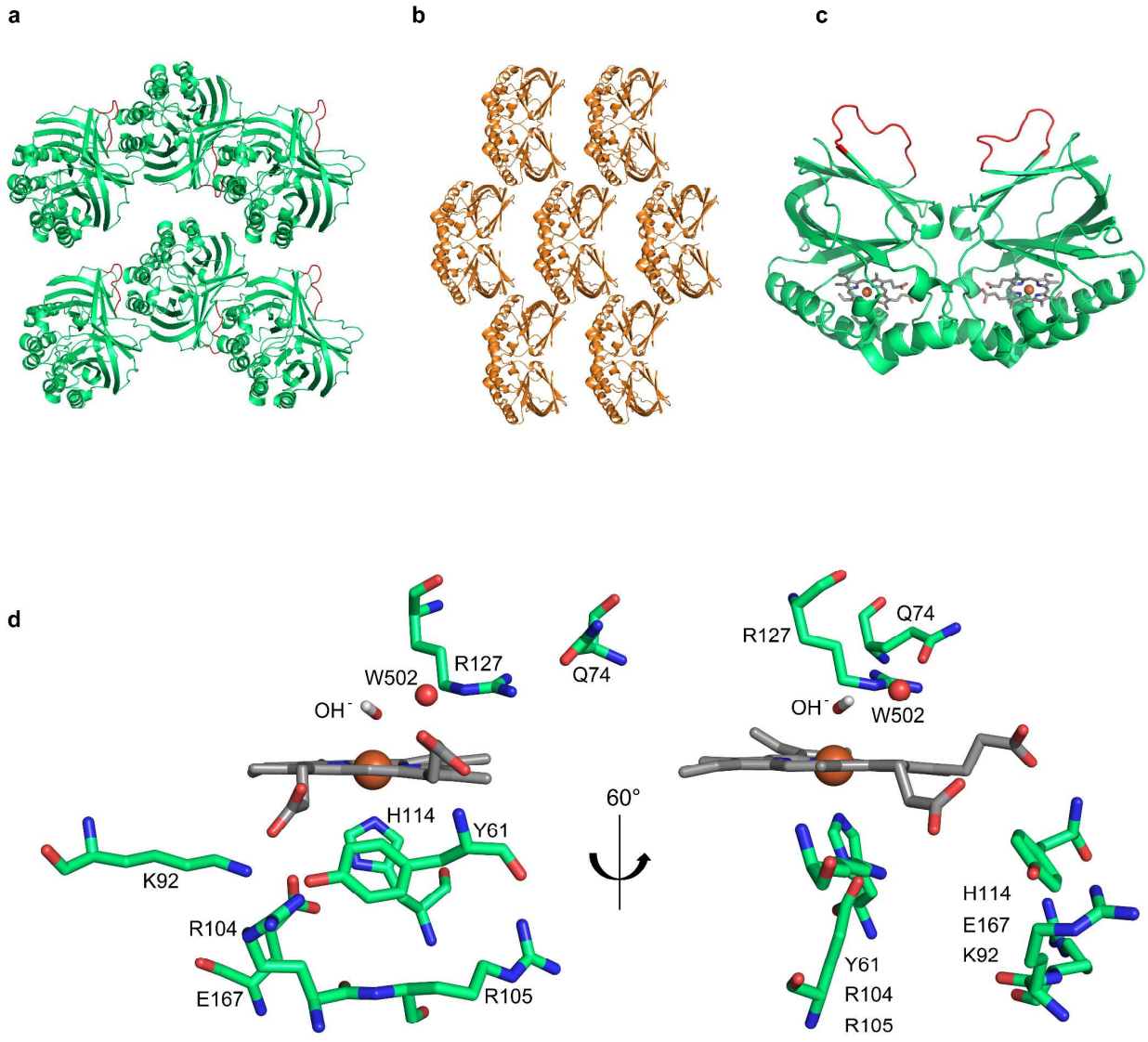

Figure S12. (a, b) Comparison of crystal packing of CCld at pH 8.5 and pH 6.5, respectively. **(c)** Structure of CCld crystallized at pH 8.5 (i.e. attenuated activity) shown as cartoon. Heme groups are depicted as grey sticks, the heme iron is shown as orange sphere. Loops shown in blue could be resolved due to altered crystal packing. **(d)** Active site of CCld crystallized at pH 8.5. Left: Detailed view of the active site surrounding amino acid residues. Distal residues include Q74 and R127, proximal residues include H114, E167, K92, Y61, R104 and R105. Waters (W) and heme iron are depicted as red and orange spheres, respectively. The heme is shown as grey sticks. The heme ligand OH^- is depicted as sticks. Right: Active site view rotated by 60° for better visualization of the separation of the proximal hydrogen bonding networks.

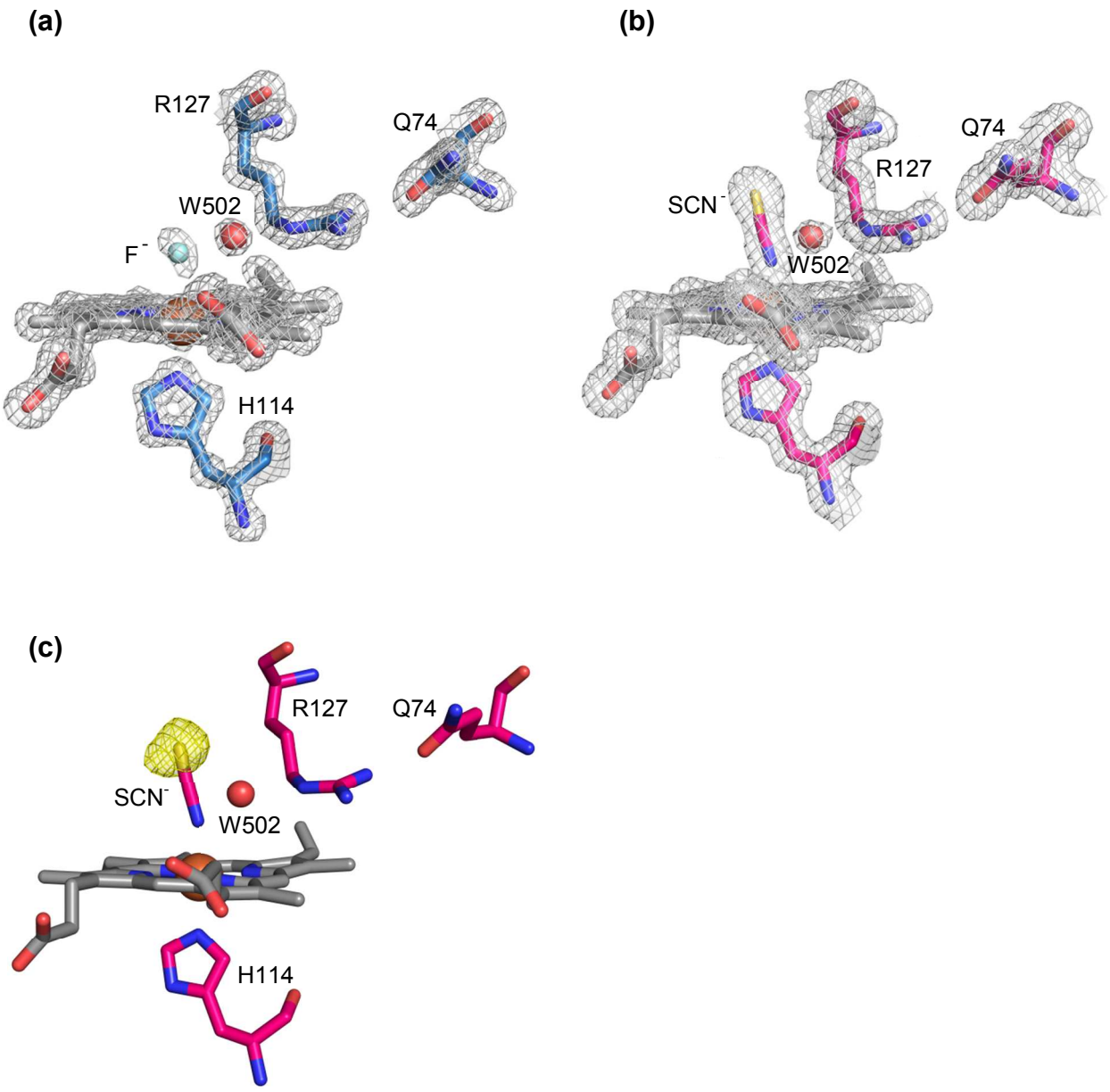

Figure S13. Stick representation of the active site of the fluoride **(a)** and isothiocyanate **(b)** complexes of CCld. Oxygen, nitrogen and sulfur atoms are colored in red, blue and yellow, respectively. Waters (W), heme iron and fluoride (F-) are depicted as red, orange and light blue spheres, respectively. Isothiocyanate (SCN^-) is depicted as a stick. The electron density (2Fo-Fc contoured at (a) σ=1.6 and (b) σ=1.7) is shown in grey. **(c)** Active site of CCld in complex with isothiocyanate. Anomalous data was collected at 1.9 Å. The calculated anomalous map for the sulphur atom is shown as yellow mesh (σ=1.7).

S3 Supporting Tables

Table S1. Band fitting parameters and band assignment in the low frequency region at alkaline pH.

RR frequency (cm^{-1})	Bandwidth (cm^{-1})	Mode assignment
472	13	
482	13	ν_{33} B_{2g}
489.5	18	ν_{22} E_g
485 (-8, -20)[a]	13	ν (FeOH) HS
507	17	ν_{12} B_{1g}
510 (-11, -22)[a]	13	ν (FeOH) LS
518	13	ν_{25} A_{2g}

[a]In parentheses are reported the isotopic shifts in D_2O and $H_2{}^{18}O$, respectively.

Table S2. RR frequencies of the Fe-Ligand frequencies

ν(Fe-L)		CCld[a]
ν(Fe-OH) LS[b]	pH 9.6	510 (-11, -22) [-11, -21]
ν(Fe-OH) HS[b]	pH 9.6	485 (-8, -20) [-10, -20]
ν(Fe-Im)	pH 5.8-9.8	231
ν(Fe-CO), ν(CO)	pH 5.8-9.8	492 (489), 1952 (1908)
ν(Fe-F)	pH 5.8	381

[a] The shifts observed for the isotopically labeled forms are reported in parentheses.

[b] The theoretical isotopic shifts calculated using the diatomic harmonic oscillator model are reported in square brackets.

Table S3. Data collection and refinement statistics for CCld at pH 6.5, pH 8.5 and in complex with fluoride. Paired refinement was used to determine the high resolution cutoff. Statistics for the high resolution shell are shown in parentheses.

	H_2O (pH 6.5)	**OH^- (pH 8.5)**	**F^-**
Wavelength (Å)	1.00	0.87	0.98
Resolution range (Å)	46.38 - 1.30 (1.35 - 1.30)	41.65 - 1.55 (1.61 - 1.55)	46.34 - 1.18 (1.22 - 1.18)
Space group	*P*1	$P12_11$	*P*1
Unit cell	51.12, 52.65, 54.73 107.2, 99.2, 108.9	54.86, 72.83, 112.49 90.0, 94.6, 90.0	51.15, 54.70, 94.27 99.1, 94.8, 99.0
Total reflections	787035 (78390)	543742 (49724)	1077657 (102955)
Unique reflections	115659 (11216)	127776 (12743)	294532 (28363)
Multiplicity	6.8 (7.0)	4.3 (3.9)	3.7 (3.6)
Completeness (%)	95.0 (91.8)	99.7 (99.8)	90.3 (86.9)
$I/\sigma(I)$	10.6 (1.0)	6.2 (0.9)	6.7 (1.0)
Wilson B-factor	17.4	15.1	15.1
R_{merge}	0.081 (2.070)	0.148 (1.210)	0.061 (1.187)
R_{meas}	0.087 (2.236)	0.170 (1.403)	0.072 (1.391)
R_{pim}	0.033 (0.838)	0.081 (0.697)	0.037 (0.719)
$CC_{1/2}$	0.998 (0.405)	0.996 (0.247)	0.997 (0.751)
CC*	1.000 (0.759)	0.999 (0.630)	0.999 (0.926)
Reflections used in refinement	115590 (11178)	127613 (12735)	294039 (28346)
Reflections used for R_{free}	1987 (193)	1311 (126)	14735 (1406)
R_{work}	0.147 (0.339)	0.198 (0.346)	0.190 (0.384)
R_{free}	0.176 (0.357)	0.228 (0.361)	0.222 (0.396)
CC(work)	0.97 (0.730)	0.965 (0.462)	0.967 (0.654)
CC(free)	0.963 (0.771)	0.962 (0.394)	0.963 (0.670)
No. of non-hydrogen atoms ***macromolecules*** ***ligands*** ***solvent***	3563 2956 109 498	7010 6012 208 790	7101 5910 210 981
protein residues	346	724	699
RMS(bonds)	0.017	0.005	0.023
RMS(angles)	1.5	0.7	2.1
Ramachandran favored (%)	98.22	96.93	98.10
Ramachandran allowed (%)	1.78	2.79	1.90
Ramachandran outliers (%)	0.00	0.28	0.00
Rotamer outliers (%)	0.33	0.00	0.00
Clashscore	1.81	1.46	1.98
Average B-factor **macromolecules** **ligands** **solvent**	25.7 23.5 22.1 39.5	26.8 26.5 18.0 30.9	21.4 19.4 18.1 34.1
Number of TLS groups	n/a	n/a	n/a

Table S4. Data collection and refinement statistics for CCld in complex with isothiocyanate and at pH 9.0 (neutron diffraction and X-ray diffraction at room temperature, respectively). Paired refinement was used to determine the high resolution cutoff. Statistics for the high resolution shell are shown in parentheses.

	SCN^-	Neutron	X-ray (room temperature)
Wavelength (Å)	0.78	2.00 - 4.00	1.54
Resolution range (Å)	46.06 - 1.28 (1.33 - 1.28)	17.22 - 2.35 (2.43 - 2.35)	19.49 - 2.00 (2.07 - 2.00)
Space group	*P*1	*P*1	*P*1
Unit cell	51.76, 54.63, 94.10 99.8, 94.8, 99.2	52.43, 53.02, 55.34 107.3, 98.5, 109.9	52.43, 53.02, 55.34 107.3, 98.5, 109.9
Total reflections	434914 (42569)	37654 (1728)	114815
Unique reflections	242310 (23676)	14292 (1065)	27988 (1457)
Multiplicity	1.8 (1.8)	2.6 (1.6)	2.6 (2.7)
Completeness (%)	93.4 (91.4)	66.7 (49.8)	80.6 (42.1)
$I/\sigma(I)$	5.0 (0.3)	7.7 (2.5)	5.6 (2.1)
Wilson B-factor	15.2	33.2	25.7
R_{merge}	0.077 (2.588)	0.20 (0.32)	0.08 (0.31)
R_{meas}	0.108 (3.660)	0.24 (0.41)	0.11 (0.38)
R_{pim}	0.077 (2.588)	0.12 (0.26)	0.06 (0.22)
$CC_{1/2}$	0.997 (0.151)	n/a	0.99 (0.82)
CC*	0.999 (0.513)	n/a	n/a
Reflections used in refinement	239834 (23541)	14292 (1065)	27983 (1458)
Reflections used for R_{free}	11852 (1150)	662 (47)	1307 (66)
R_{work}	0.210 (0.478)	0.239 (0.400)	0.140 (0.144)
R_{free}	0.236 (0.491)	0.253 (0.400)	0.186 (0.192)
CC(work)	0.953 (0.293)	n/a	n/a
CC(free)	0.947 (0.365)	n/a	n/a
No. of non-hydrogen atoms ***macromolecules*** ***ligands*** ***solvent***	6866 5816 249 801	3152 2947 95 110	3152 2947 95 110
protein residues	1082	357	357
RMS(bonds)	0.015	0.025	0.025
RMS(angles)	1.4	2.0	2.0
Ramachandran favored (%)	97.65	97.13	97.13
Ramachandran allowed (%)	2.35	2.58	2.58
Ramachandran outliers (%)	0.00	0.29	0.29
Rotamer outliers (%)	0.17	3.93	3.93
Clashscore	2.25	4.85	4.85
Average B-factor **macromolecules** **ligands** **solvent**	26.0 25.1 24.9 32.3	56.0 56.6 37.6 55.7	56.0 56.6 37.6 55.7
Number of TLS groups	n/a	2	2

S4 References

(1) Schaffner, I.; Hofbauer, S.; Krutzler, M.; Pirker, K. F.; Bellei, M.; Stadlmayr, G.; Mlynek, G.; Djinovic-Carugo, K.; Battistuzzi, G.; Furtmüller, P. G.; Daims, H.; Obinger, C. *Mol. Microbiol.* **2015**, *96*, 1053-1068.
(2) Kabsch, W. *Acta Crystallogr., Sect. D: Biol. Crystallogr.* **2010**, *66*, 125-132.
(3) Adams, P. D.; Afonine, P. V.; Bunkoczi, G.; Chen, V. B.; Davis, I. W.; Echols, N.; Headd, J. J.; Hung, L. W.; Kapral, G. J.; Grosse-Kunstleve, R. W.; McCoy, A. J.; Moriarty, N. W.; Oeffner, R.; Read, R. J.; Richardson, D. C.; Richardson, J. S.; Terwilliger, T. C.; Zwart, P. H. *Acta Crystallogr., Sect. D: Biol. Crystallogr.* **2010**, *66*, 213-221.
(4) Emsley, P.; Lohkamp, B.; Scott, W. G.; Cowtan, K. *Acta Crystallogr., Sect. D: Biol. Crystallogr.* **2010**, *66*, 486-501.
(5) Chen, V. B.; Arendall, W. B., 3rd; Headd, J. J.; Keedy, D. A.; Immormino, R. M.; Kapral, G. J.; Murray, L. W.; Richardson, J. S.; Richardson, D. C. *Acta Crystallogr., Sect. D: Biol. Crystallogr.* **2010**, *66*, 12-21.
(6) Joosten, R. P.; Salzemann, J.; Bloch, V.; Stockinger, H.; Berglund, A. C.; Blanchet, C.; Bongcam-Rudloff, E.; Combet, C.; Da Costa, A. L.; Deleage, G.; Diarena, M.; Fabbretti, R.; Fettahi, G.; Flegel, V.; Gisel, A.; Kasam, V.; Kervinen, T.; Korpelainen, E.; Mattila, K.; Pagni, M.; Reichstadt, M.; Breton, V.; Tickle, I. J.; Vriend, G. *J. Appl. Crystallogr.* **2009**, *42*, 376-384.
(7) Karplus, P. A.; Diederichs, K. *Science* **2012**, *336*, 1030-1033.
(8) DeLano, W. L. *The PyMOL Molecular Graphics System on World Wide Web*, **2000**, http://www.pymol.org.
(9) Ng, J. D.; Baird, J. K.; Coates, L.; Garcia-Ruiz, J. M.; Hodge, T. A.; Huang, S. J. *Acta Crystallogr., Sect. F: Struct. Biol. Commun.* **2015**, *71*, 358-370.
(10) Coates, L.; Cuneo, M. J.; Frost, M. J.; He, J. H.; Weiss, K. L.; Tomanicek, S. J.; McFeeters, H.; Vandavasi, V. G.; Langan, P.; Iverson, E. B. *J. Appl. Crystallogr.* **2015**, *48*, 1302-1306.
(11) Coates, L.; Stoica, A. D.; Hoffmann, C.; Richards, J.; Cooper, R. *J. Appl. Crystallogr.* **2010**, *43*, 570-577.
(12) Arnold, O.; Bilheux, J. C.; Borreguero, J. M.; Buts, A.; Campbell, S. I.; Chapon, L.; Doucet, M.; Draper, N.; Leal, R. F.; Gigg, M. A.; Lynch, V. E.; Markyardsen, A.; Mikkelson, D. J.; Mikkelson, R. L.; Miller, R.; Palmen, K.; Parker, P.; Passos, G.; Perring, T. G.; Peterson, P. F.; Ren, S.; Reuter, M. A.; Savici, A. T.; Taylor, J. W.; Taylor, R. J.; Tolchenoy, R.; Zhou, W.; Zikoysky, J. *Nucl. Instrum. Methods Phys. Res., Sect. A* **2014**, *764*, 156-166.
(13) Campbell, J. W.; Hao, Q.; Harding, M. M.; Nguti, N. D.; Wilkinson, C. *J. Appl Crystallogr.* **1998**, *31*, 496-502.
(14) Afonine, P. V.; Mustyakimov, M.; Grosse-Kunstleve, R. W.; Moriarty, N. W.; Langan, P.; Adams, P. D. *Acta Crystallogr., Sect. D: Biol. Crystallogr.* **2010**, *66*, 1153-1163.
(15) Adams, P. D.; Mustyakimov, M.; Afonine, P. V.; Langan, P. *Acta Crystallogr., Sect. D: Biol. Crystallogr.* **2009**, *65*, 567-573.
(16) Battistuzzi, G.; Bellei, M.; Vlasits, J.; Banerjee, S.; Furtmüller, P. G.; Sola, M.; Obinger, C. *Arch. Biochem. Biophys.* **2010**, *494*, 72-77.
(17) Battistuzzi, G.; Bellei, M.; Zederbauer, M.; Furtmüller, P. G.; Sola, M.; Obinger, C. *Biochemistry* **2006**, *45*, 12750-12755.
(18) Battistuzzi, G.; Borsari, M.; Ranieri, A.; Sola, M. *J. Am. Chem. Soc.* **2001**, *124*, 26-27.
(19) Morris, J. C. *J. Phys. Chem.* **1966**, *70*, 3798-3805.
(20) Piovesan, D.; Minervini, G.; Tosatto, S. C. *Nucleic Acids Res.* **2016**, *44*, W367-374.